Registration Based SIRT: A reconstruction algorithm for 4D CT

Vincent Van Nieuwenhove[1], Jan De Beenhouwer[1], Jelle Vlassenbroeck[2], Maarten Moesen[3], Mark Brennan[3], Jan Sijbers[1]

[1]University of Antwerp, Universiteitsplein 1, Wilrijk, Belgium, e-mail: Vincent.VanNieuwenhove@uantwerpen.be, Jan.DeBeenhouwer@Uantwerpen.be, Jan.Sijbers@uantwerpen.be

[2]Inside Matters, Meet District bus 502, Ottergemsesteenweg Zuid 808, Ghent, Belgium, e-mail: jelle@insidematters.eu

[3]Huntsman, Everslaan 45, Everberg, Belgium, e-mail: Maarten_Moesen@Huntsman.com, Mark_Brennan@Huntsman.com

Abstract

The goal of 4D computed tomography (4D CT) is to study the temporal deformation of a 3D sample with a sufficiently high temporal and spatial resolution. Conventionally, the sample is sequentially scanned, resulting in datasets of successive time frames. Each of these datasets is then independently reconstructed. This framework results in a trade-off between the temporal resolution and the signal-to-noise ratio (SNR) of the reconstructed images. The proposed registration based simultaneous iterative reconstruction technique (RBSIRT) allows shortening the acquisition time per time frame, leading to improved temporal resolution at comparable SNR. To this end, the algorithm estimates the deformation field between different time frames, which allows incorporating projections of other time frames into the reconstruction of a particular time frame. The technique was validated on numeric simulations and on a real dynamic experiment of a polyurethane foam sample. The reconstructions obtained with RBSIRT have a significantly higher SNR compared to the SNR of conventional 4D reconstructions.

Keywords: 4D CT, dynamic, reconstruction algorithm, computed tomography, image registration

1 Introduction

4D (3 spatial dimensions + time) computed tomography (CT) has the ability to image dynamic processes in a non-destructive manner. This technique has great potential for validating models of dynamic processes, e.g. the compression of polyurethane (PU) foam [1].

In dynamic CT, conventionally, several CT datasets (time frames) are acquired sequentially. Each time frame typically consists of a set of projections acquired over an angular range of 180 or 360 degrees. Afterwards, these time frames are independently reconstructed [2]. However, due to the long acquisition time of conventional micro-CT, two problems arise if a fast dynamic process is imaged. Firstly, the long acquisition time of a single time frame strongly limits the temporal resolution. Secondly, due the object deformation during the acquisition of a single time frame, the reconstructed images are blurry due to deformation artefacts. A straight forward method to avoid both problems is shortening the acquisition time of a single time frame. This can be achieved by shortening the integration time of a single projection or lowering the number of projections per time frame. A shorter integration time reduces the signal-to-noise ratio (SNR) of the projection data which in turn leads to a lower SNR in the reconstructed images. Lowering the number of projections, on the other hand, results in streaks in the reconstructed images, often referred to as sub-sampling artefacts. As a result the conventional workflow leads to a trade-off between the temporal resolution/deformation artefacts and low SNR/sub-sampling artefacts in the reconstructed images.

However, this trade-off can be improved by exploiting data redundancy present in 4D CT datasets. Since in every time frame the same, though slightly changed, object is scanned, it is beneficial to include information about other time frames into the reconstruction process [3]. In this work, the object's dynamics is modeled through a deformation vector field (DVF). This vector field describes the displacement of every voxel between two time frames. The proposed registration based simultaneous reconstruction technique (RBSIRT) incorporates these deformation fields into the reconstruction process, as such enabling the incorporation of the projections of other time frames into the reconstruction. Unfortunately, the DVF's are unknown and need to be estimated. In order to estimate these, volume registrations are performed on conventionally reconstructed volumes of the different time frames.

In section 2 the proposed reconstruction algorithm and deformation estimation strategy will be explained. Our method will be compared with other reconstruction algorithms in a numerical way as well as on an experimental dataset as explained in section 3. The results of these experiments are then discussed in section 4.

2 Methods

The proposed RBSIRT workflow consists of two main parts. The first part estimates the deformation between the different time frames. The RBSIRT reconstruction algorithm then exploits these deformation estimations to calculate a high SNR reconstruction. In subsection 2.1, an overview of the conventional Simultaneous Iterative Reconstruction Technique (SIRT) algorithm will be given. The SIRT algorithm is a well-known algebraic reconstruction algorithm for conventional (stationary)

CT. Next, in subsection 2.2, the RBSIRT reconstruction algorithm, which is based on the SIRT algorithm, will be introduced. Lastly, in subsection 2.3, an estimation method for the deformation vector fields is introduced.

2.1 Simultaneous Iterative Reconstruction Technique

Let $\boldsymbol{x} = (x_k) \in \mathbb{R}^N$ represents the voxel values of the unknown volume. The (log-corrected) projections are represented by $\boldsymbol{p} = (p_k) \in \mathbb{R}^M$. The system matrix $\boldsymbol{A}$ contains the contributions of each voxel to each detector element. As such, the projections can be simulated with $\boldsymbol{Ax} \cong \boldsymbol{p}$. This system of equations cannot be solved directly for $\boldsymbol{x}$ since it is ill-defined. Therefore, the SIRT algorithm solves following optimization problem: $\boldsymbol{x}^* = \text{argmin}_x \|\boldsymbol{Ax} - \boldsymbol{p}\|_R$, where $\|\boldsymbol{Ax} - \boldsymbol{p}\|_R = (\boldsymbol{Ax} - \boldsymbol{p})^T \boldsymbol{R}(\boldsymbol{Ax} - \boldsymbol{p})$ and $\boldsymbol{R} = (r_{kl}) \in \mathbb{R}^{M \times M}$ is a diagonal matrix with $r_{kk} = 1/\sum_l a_{kl}$ [4]. The following iterative formula is known to converge to this minimum:

$$\boldsymbol{x^{k+1}} = \boldsymbol{x^{(k)}} + \boldsymbol{CA}^T \boldsymbol{R}\left(\boldsymbol{p} - \boldsymbol{Ax^k}\right)$$

where $\boldsymbol{C} = (c_{kl}) \in \mathbb{R}^{N \times N}$ is a diagonal matrix with $c_{ll} = 1/\sum_k a_{kl}$. The reconstruction accuracy of this method greatly depends on the dimensionality of the null space of the matrix $\boldsymbol{A}$. By adding more projections (more linear equations) to the problem the dimensionality of this null space can be reduced, yielding better results. In the following subsection transformations between time points will be incorporated into the SIRT algorithm. As such, projections of other time points can be included into the reconstruction process without causing deformation artefacts.

2.2 Registration based SIRT

The reconstructed object at time frame r can be represented as a column vector $\boldsymbol{x_r} = (x_{r,k}) \in \mathbb{R}^N$. The vector $\boldsymbol{p_r} = (p_{r,k}) \in \mathbb{R}^{M_r}$ denotes all the acquired projections of the object at time frame r. The projections are simulated with the forward model: $\boldsymbol{p_r} = \boldsymbol{A_r}\, \boldsymbol{x_r}$, where $\boldsymbol{A_r} = (a_{r,kl}) \in \mathbb{R}^{M_r \times N}$. To reconstruct the object at time frame r, we propose the following SIRT [4] based iterative reconstruction algorithm:

$$\boldsymbol{x_r^{k+1}} = \boldsymbol{x_r^{(k)}} + \sum_{r'} w_{rr'} \tau_{r \to r'}^{-1} \boldsymbol{C}_{r'} \boldsymbol{A}_{r'}^T \boldsymbol{R}_{r'} \left(\boldsymbol{p}_{r'} - \boldsymbol{A}_{r'} \tau_{r \to r'} \boldsymbol{x_r^k}\right) \quad (1)$$

where $\boldsymbol{C_r} = (c_{r,kl}) \in \mathbb{R}^{N \times N}$ is a diagonal matrix with $c_{r,ll} = 1/\sum_k a_{r,kl}$ and $\boldsymbol{R_r} = (r_{r,kl}) \in \mathbb{R}^{M_r \times M_r}$ is a diagonal matrix with $r_{r,kk} = 1/\sum_l a_{r,kl}$. The operator $\tau_{r \to r'}$ transforms the object at time frame r to its state at time frame r': $\boldsymbol{x_{r'}} = \tau_{r \to r'} \boldsymbol{x_r}$. The weights $w_{rr'}$ are normalized such that $\sum_{r'} w_{rr'} = 1$. For each time frame r', the proposed reconstruction algorithm transforms the current estimate of $\boldsymbol{x_r}$ to the r''th time frame and then calculates a SIRT update using the projection data of time frame r'. This SIRT update is then transformed back to time frame r, weighted with $w_{r'}$ and added to the current total update of $\boldsymbol{x_r^k}$. This is repeated for all time frames after which the total update is added to $\boldsymbol{x_r^k}$. An overview of a single RBSIRT iteration is given in figure 1.

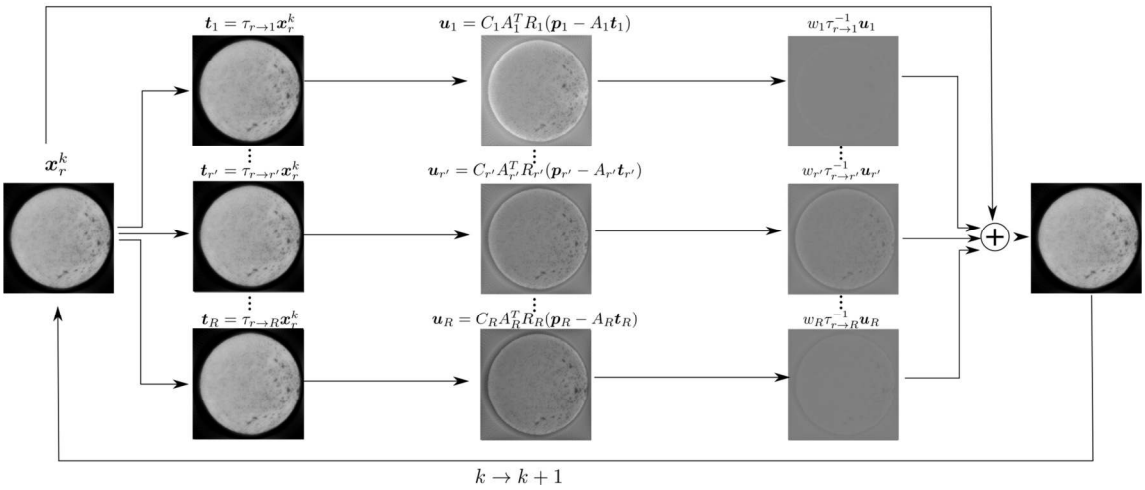

Figure 1: Schematic representation of a single iteration of the registration based SIRT algorithm

2.2 Deformation estimation

The deformation operators $\tau_{r \to r'}$ and their inverse (see Eq. (1)) are unknown and have to be estimated. To this end, each time frame is first conventionally reconstructed with SIRT using only the projections corresponding to that time frame. Afterwards, these conventional reconstructions $(\boldsymbol{c_1}, \boldsymbol{c_2}, \ldots, \boldsymbol{c_R})$ are pairwise registered with each other, resulting in deformation vector fields (DVFs). The registration, performed with the registration software Elastix [5], estimates the parameters $\boldsymbol{\alpha}_{rr'}$ of a B-spline deformation model [6]. The inverse DVFs are calculated as described in Chen et al. [7]. The weights $w_{rr'}$ reflect the accuracy of the corresponding DVFs and are calculated as follows:

$$w_{rr\prime} = e^{-\left(\frac{k_{rr\prime}}{q}\right)^2} / \sum_l e^{-\left(\frac{k_{rl}}{q}\right)^2}$$

where $k_{rr'} = \frac{1}{N}\sum_i \left(c_{r,i} - (\tau(\boldsymbol{\alpha}_{rr'})\boldsymbol{c}_{r\prime})_i\right)^2$ corresponds to the mean squared distance (MSD) between the reconstructed time frame and the transformed reconstruction of the time frame r'. The parameter q regulates the magnitude of the weights.
The proposed method was implemented in Matlab, the forward and back projections were performed with the ASTRA toolbox [8]. We will refer to the reconstruction algorithm as RBSIRT. An overview of the complete method is shown in figure 2.

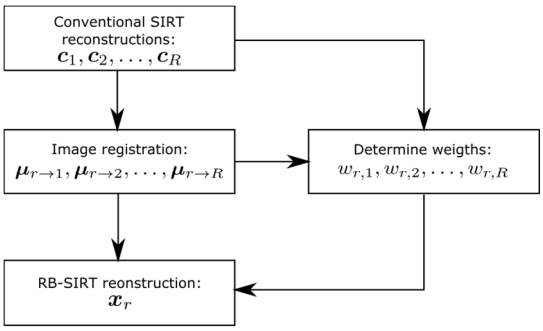

Figure 2: Schematic representation of the full RBSIRT reconstruction pipeline.

3 Experiments

The RBSIRT method was compared to several other methods in numerical simulations (subsection 3.1) and on an experimental dataset of polyurethane foam under compression (subsection 3.2). The results of these experiments are discussed in section 4.

3.1 Numerical simulations

Several numerical experiments were performed on a numerical phantom of PU foam under compression. These models were provided by Huntsman (Everberg, Belgium) and are based on finite element simulations of different stages in the compression process. Four models were voxelised on an isotropic voxel grid of $400 \times 400 \times 400$ from which 100×100 pixel projections were generated, in order to avoid the "inverse crime" of generating the data with the same model as the model used in the reconstruction [9]. The projections were simulated in an interleaved scanning protocol with 20 projections per time frame, where each time frame has an angular range of 180 degrees [10]. Poisson distributed noise was applied on the data, assuming an incoming beam intensity of 10^4 (photon count). During each time frame the foam was compressed another 1,75% of the original sample height.
The sample was reconstructed with a range of different reconstruction techniques:

- **FDK:** The Feldkamp-David-Kress (FDK) algorithm applied on each rotation independently [11].
- **FDKmean:** A straight forward method to improve the FBP reconstructions. In a first step the FDK reconstructions are registered to one another. The estimated deformations are then applied on the reconstructions of the other time points and a weighted mean of the reconstructions is calculated.
- **SIRT:** the SIRT algorithm applied on each rotation independently.
- **SIRTmean:** The same concept as FBPmean, but this time with the SIRT reconstructions.
- **RBSIRT:** The method described in the method section starting from a zero image.
- **RBSIRTinit:** The method described in the method section initialized with the result of SIRTmean.

The volume registration was performed with a b-spline deformation model with a control point spacing of 8 voxels. The b-spline parameters were optimized by minimizing the mean squared difference in a multi-resolution framework.
The SIRT, RBSIRT and RBSIRTinit algorithms were iterated until the lowest Mean Squared Error (MSE) was achieved. The optimal value of the parameter q, in terms of the MSE of the reconstructions, was 0.8 and was selected in this experiment.
Renderings of the different reconstructions are shown in figure 3.
Both the Structural Similarity Index and the MSE of the reconstructions were calculated in function of the photon count and the number of projections per time frame [12]. These results are shown in figure 4 and figure 5, respectively.

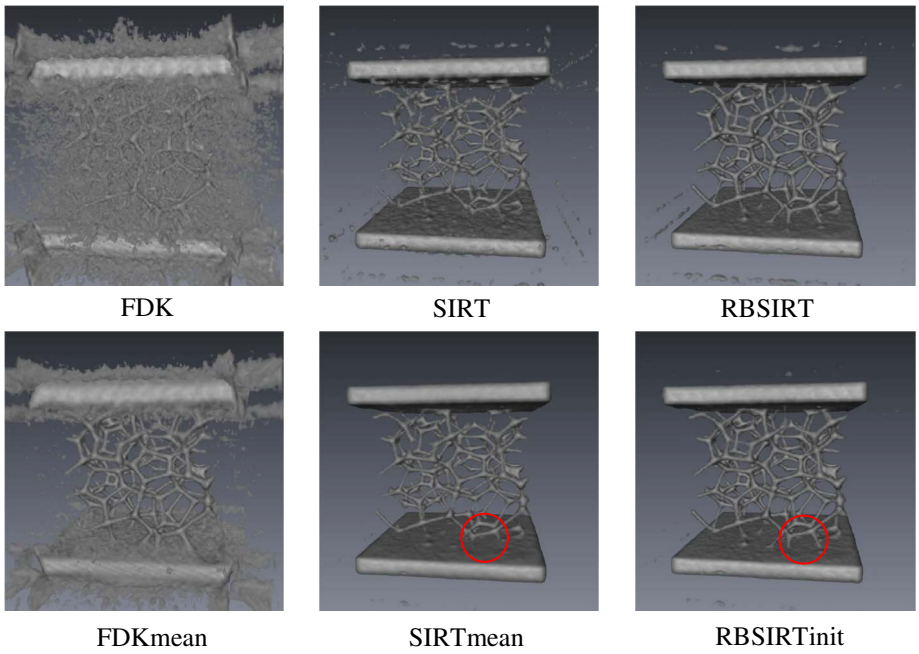

Figure 3: Renderings of the reconstruction of the numerical simulation of the compression of a foam sample with different reconstruction techniques (detailed description section 3.1). The red circles indicate example areas where the struts that are better reconstructed in the RBSIRT reconstructions in comparison with the SIRTmean reconstruction.

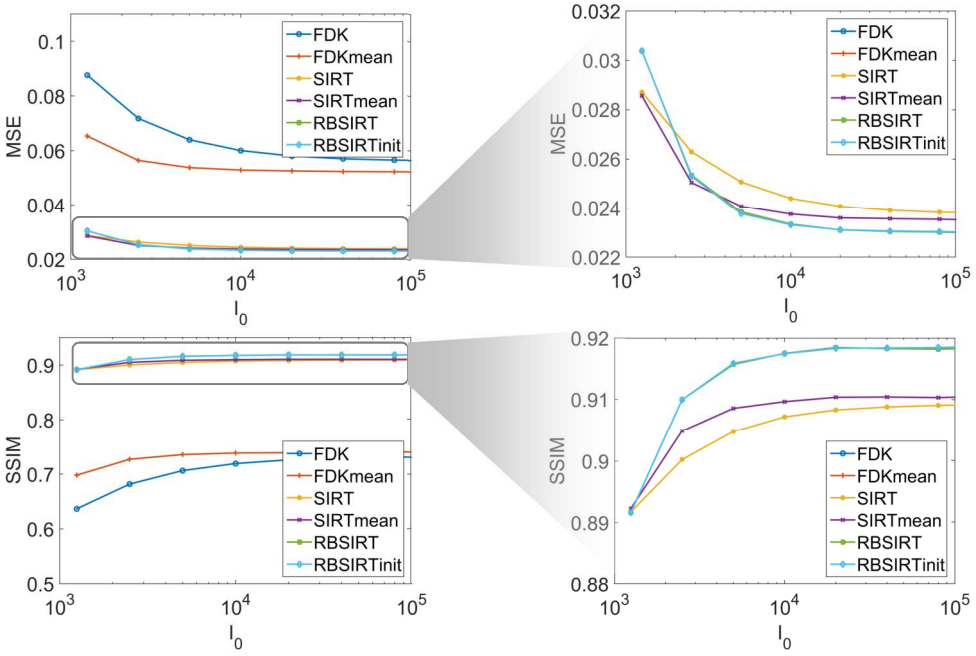

Figure 4: MSE and SSIM in function of the incoming photon count. Top left: mean squared error in function of the photon count. Top right: zoomed in version of the top left image. Bottom left: SSIM in function of the photon count. Bottom right: zoomed in version of the bottom left image.

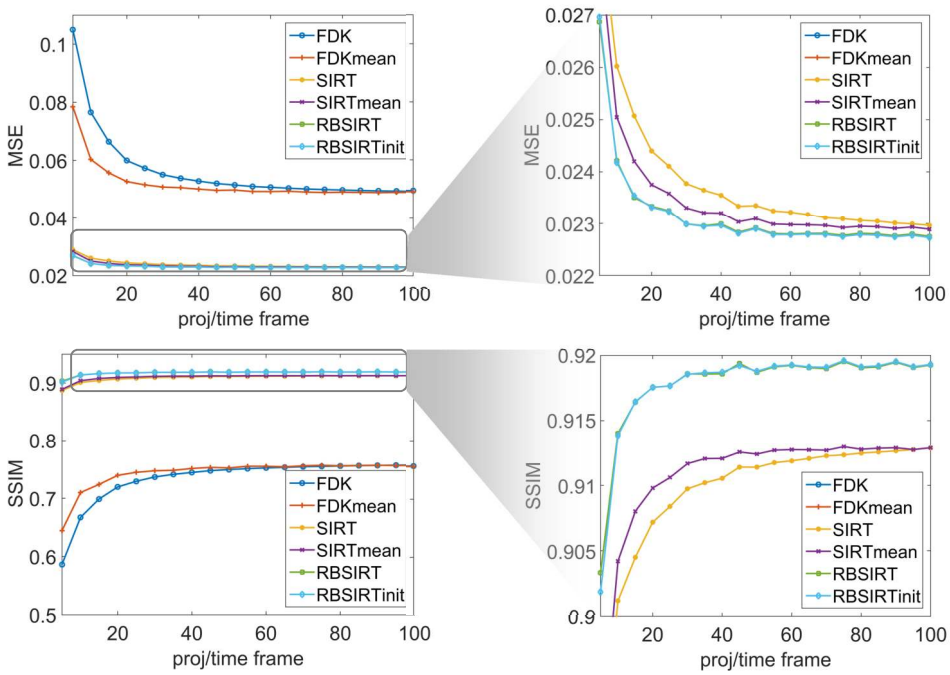

Figure 5: MSE and SSIM in function of the number of projections per time frame. Top left: mean squared error in function of the number of projections. Top right: zoomed in version of the top left image. Bottom left: SSIM in function of the number of projections. Bottom right: zoomed in version of the bottom left image.

3.2 Polyurethane dataset

A dynamic x-ray CT dataset was acquired by Inside Matters with a gantry-based high-resolution scanner [13]. A polyurethane foam sample (provided by Huntsman) of 11mm high was loaded in a compression stage which was mounted in the scanner. Seven CT datasets were acquired. Each dataset (= time frame) consists out of 2000 equiangular projections (1316 ×1312 pixels, pixel size 0.1 mm) acquired over an angular range of 360 degrees. During these scans the sample was compressed $l \cdot 0.5\ mm$, where l=0,..,L-1 is the time frame number. All reconstructions were calculated on a 1316x1316x401 isotropic voxel grid with a voxel size of 16μm.

Each time frame was reconstructed with three different methods: Firstly, conventional SIRT with 2000 projections/time frame. Secondly, conventional SIRT with 1000 projections/time frame and, thirdly, RBSIRTinit with 1000 projections/time frame. RBSIRT estimates the deformation and includes the projections of a single neighbouring time frame to the reconstruction of a particular time frame. The SIRT reconstruction with 2000 projections has thus the best possible quality that the RBSIRT reconstruction can achieve by incorporating the projections of a single neighbouring time frame. Reconstructions with only 1000 projections were performed with projections with projection numbers $1 + (l \bmod 2), 3 + (l \bmod 2), \ldots, N$, where l is the time frame number and N the total number of acquired projections/time frame. As such neighbouring time frames have interleaved projections. The volume registration was performed with a b-spline deformation model with a control point spacing of 8 voxels. The b-spline parameters were optimized by minimizing the mean squared difference in a multi-resolution framework. The RBSIRTinit reconstruction was initialized as described in section 3.1 after which 50 RBSIRT iterations were performed.

In figure 6, a slice, reconstructed with the three methods described above, of the third time frame are shown. This figure also shows zoomed reconstructions and a segmentation of each reconstruction performed with Otsu's method [14].

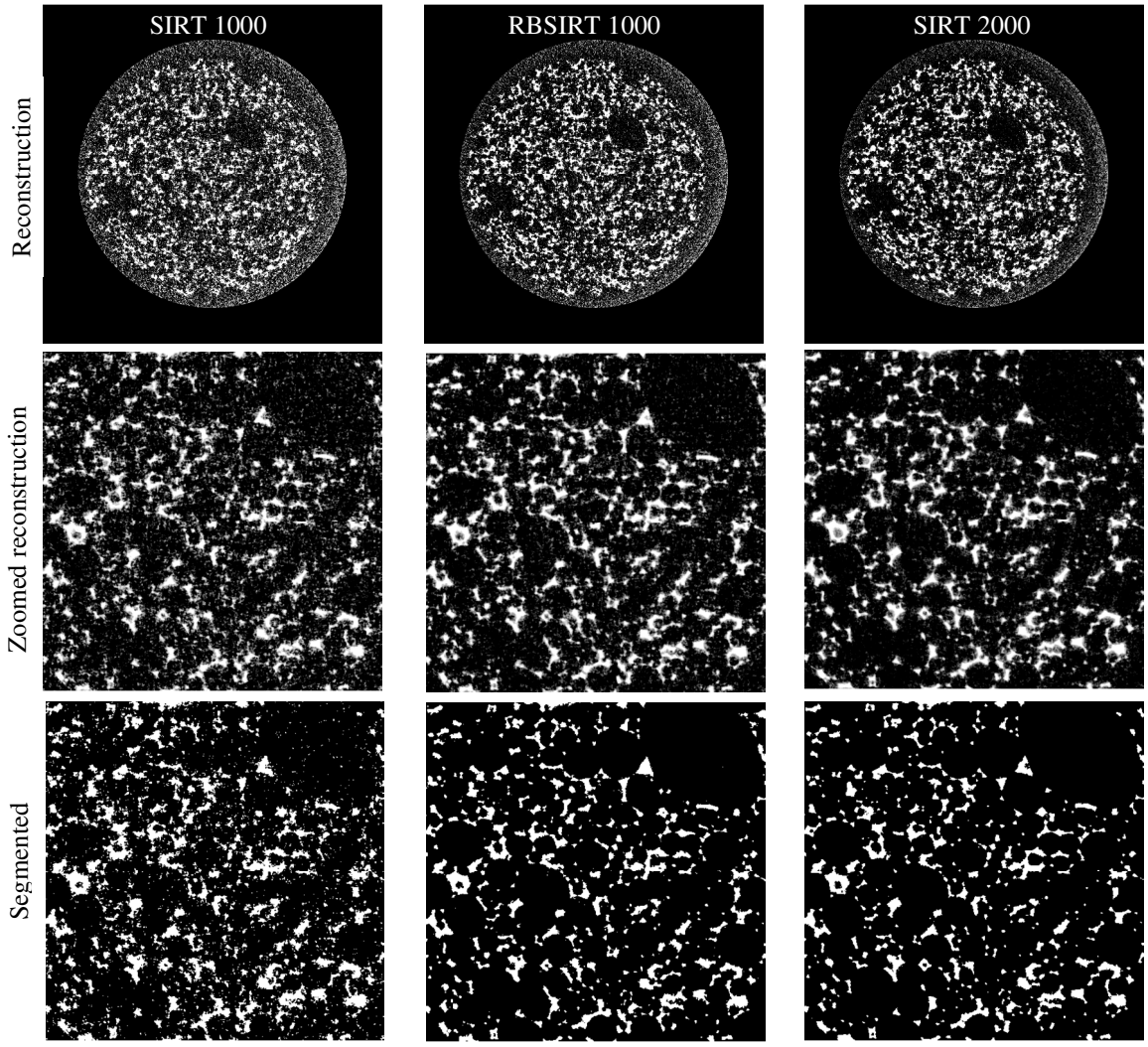

Figure 6: Reconstructions (top), zoomed reconstructions (middle) and segmentations (bottom) of the 3th time frame of the polyurethane dataset. Left: SIRT with 1000 proj/time frame. Middle: RBSIRTinit with 1000 proj/time frame. Right: SIRT with 2000 proj/time frame.

4 Discussion

In this section, the results of the numerical simulations and the polyurethane dataset will be discussed.

4.1 Numerical simulations

Figure 3 shows renderings of the second time frame of the compressed foam sample calculated with the different reconstruction techniques explained in section 3.1. FDK produces the worst results. The reconstruction is very noisy and the foam structures are very hard to differentiate from their surroundings. The FDKmean algorithm improves this reconstruction significantly, however high levels of noise are still present around the pressure plates due to cone beam artefacts. The SIRT and SIRTmean reconstructions show the foam structure nicely, however some struts of the foam are missing in the neighbourhood of the pressure plates. The RBSIRT and RBSIRTinit reconstructions show the foam structure clearly and are able to reconstruct the struts close to the pressure plate better than the SIRT and SIRTmean reconstructions (see red circles in figure 3 for example regions). The RBSIRT and RBSIRTinit reconstructions are almost indistinguishable. Note that, RBSIRTinit is faster than the RBSIRT reconstruction since it needs much less RBSIRT iterations to converge to the optimal solution.

In figure 4 the MSE and SSIM in function of the photon count is shown. Both in respect of the MSE and SSIM the RBSIRT and RBSIRTinit reconstructions perform the best and almost no difference can be observed between both methods. The SIRTmean method provides slightly worse reconstruction, but is an improvement over the conventional SIRT reconstructions. Only at very low noise levels the RBSIRT methods result in slightly worse reconstructions than the SIRT methods, which is caused by inaccurate deformation estimations on the very low SNR initial SIRT reconstructions. FDK and FDKmean provide the worst results, although FDKmean clearly improves upon conventional FDK.

From figure 5, similar conclusions can be drawn. Here the RBISRT methods provide the best results with respect to the MSE and SSIM. This confirms our expectation that all results improve if more projections per time frame are provided.

4.2 Polyurethane dataset

The results of the polyurethane are shown in figure 6. The SIRT reconstruction with 2000 projections/time frame shows the foam structures very clearly. The SNR is sufficiently high to observe small foam structures. The SIRT reconstruction with only 1000 projections/time frame has a visibly lower SNR than the SIRT reconstruction with 2000 projections/time frame. High frequency components of the images are heavily degraded with noise. The RBSIRT reconstruction (1000 projections/time frame) possesses slightly lower SNR as the SIRT reconstruction with 2000 projections/time frame, however the SNR is considerably higher than that of the SIRT reconstruction with 1000 projections/time frame.
The segmented reconstructions show that the foam structures in both the RBSIRT and SIRT reconstruction with 2000 projections per time frame can be easily segmented with the Otsu segmentation algorithm. Due to noise, this isn't the case for SIRT with only 1000 projections per time frame.
These results clearly indicate that RBSIRT can achieve results with higher reconstruction quality in comparison to the SIRT reconstructions of the same 4DCT dataset. RBSIRT allows shortening the acquisition time of each time frame, by lowering the number of projections, without considerable reconstruction quality loss.

5 Conclusions

The performed experiments show that the RBSIRT algorithm is able to successfully exploit the data redundancy present in 4D CT datasets. It allows lowering the acquisition time of a single time frame without compromising the SNR of the reconstructed images. This is achieved by estimating the deformation between different time frames which allows including projections of different time frames into the reconstruction of a certain time frame without introduction of deformation artefacts. The method was validated on numerical simulations and a real dataset of polyurethane foam under compression. Both experiments showed an increase of reconstruction quality with respect to conventional reconstruction algorithms.

Acknowledgements

The authors would like to thank the Centre for X-ray Tomography of the Ghent University (UGCT) for the use of their CT facilities. This work was supported by the iMinds ICON MetroCT project and the Agency for Innovation by Science and Technology (IWT).

References

[1] J.A. Elliott, A.H. Windle, J.R. Hobdell, G. Eeckhaut, R.J. Oldman, W. Ludwig, E. Boller, P. Cloetens and J. Baruchel, In-situ deformation of an open-cell flexible polyurethane foam characterised by 3D computed micro tomography J. Mater. Sci. 37, 1547-1555, 2002.
[2] V. Cnudde and M.N. Boone, High-resolution X-ray computed tomography in geosciences: A review of the current technology and applications, Earth-Sci. Rev. 123, 1–17 , 2013.
[3] G. Van Eyndhoven, K.J. Batenburg, D. Kazantsev, V. Van Nieuwenhove, P.D. Lee, K.J. Dobson, and J. Sijbers, An iterative CT reconstruction algorithm for fast fluid flow imaging, IEEE Trans. Image Process. 24, 4446–4458, 2015.
[4] J. Gregor and T. Benson, Computational analysis and improvement of SIRT, IEEE Trans. Med. Imag. 27(7), 918-924, 2008.
[5] http://elastix.isi.uu.nl/.
[6] D. Rueckert, L. I. Sonoda, C. Hayes, D. L. G. Hill, M. O. Leach, and D. J. Hawkes. Nonrigid registration using free-form deformations: application to breast MR images. IEEE Trans. Med. Imag. 18(8), 712 – 721, 1999.
[7] M. Chen, W. Lu, Q. Chen, K.J. Ruchala, and G.H. Oliviera, A simple fixed-point approach to invert a deformation field, Med. Phys. 35(1), 81-88, 2008.
[8] W. van Aarle, W J. Palenstijn, J. Cant, E. Janssens, F. Bleichrodt, A. Dabravolski, J. De Beenhouwer, K. J. Batenburg, and J. Sijbers, Fast and flexible X-ray tomography using the ASTRA toolbox, Opt. Express 24 (22), 25129-25147, 2016
[9] J. Kaipio and E. Somersalo, Statistical inverse problems: Discretization, model reduction and inverse crime, J. Comput. Appl. Math. 198, 493-504, 2007.
[10] A. Kaestner, B. Münch, P. Trtik, L. Butler, Spatiotemporal computed tomography of dynamic processes, Opt. Eng. 50 (12), 12301, 2011
[11] L. A. Feldkamp, L. C. Davis and J. W. Kress, Practical cone-beam algorithm, J. Opt. Soc. Am. A 1, 612-619, 1984.
[12] Z. Wang, A.C. Bovik, H.R. Sheikh, E.P. Simoncelli, Image quality assessment: from error visibility to structural similarity, IEEE Trans. Image Process., 13 (4): 600–612, 2004.
[13] M. Dierick, D. Van Loo, B Masschaele, J. Van den Bulcke, J. Van Acker, V. Cnudde, and L. Van Hoorebeke, Recent micro-CT scanner developments at UGCT, Tomography of materials and structures, 9-12, 2013.
[14] N. Otsu, A threshold selection method from gray-level histograms. IEEE Trans. Sys. Man., Cyber. 9 (1), 62–66, 1979.